JOURNAL OF MATERIALS SCIENCE 29 (1994) 5559–5568

Three-dimensional interaction of crazes and micro-shearbands in PC–SAN microlayer composites

K. SUNG*, A. HILTNER‡, E. BAER
Department of Macromolecular Science and Center for Applied Polymer Research, Case Western Reserve University, Cleveland, OH 44106, USA

The three-dimensional interaction of crazes and micro-shearbands in co-extruded microlayer sheets with 49 alternating layers of polycarbonate (PC) and styrene–acrylonitrile copolymer (SAN) was investigated as a function of the relative layer thickness. The deformation processes were observed when microspecimens were deformed under an optical microscope. Deformed specimens were sectioned and examined further in the transmission electron microscope. Two types of craze were observed in the SAN layers: surface crazes initiated at a strain of about 1.8% and gradually lengthened to a maximum of 70 μm when they were arrested by micro-shearbands at 4.2% strain, while tunnel crazes appeared above 4.2% strain and rapidly grew through the entire SAN layer. Surface crazes did not prevent yielding and stable neck propagation, while tunnel crazes were responsible for fracture prior to neck formation. The density of surface crazes relative to tunnel crazes increased as the PC–SAN ratio increased or as the strain rate decreased. The surface crazes stimulated micro-shearbanding in both PC and SAN layers. After micro-shearbands initiated in the PC layers where the craze impinged on the PC–SAN interface, they propagated rapidly along the edges of the craze. As they overtook the craze tip, the micro-shearbands penetrated through the PC–SAN interface and continued around the craze tip to entirely engulf the craze. This terminated craze growth, and further strain in the SAN layer was accommodated by shear deformation.

1. Introduction

Numerous studies have examined the interaction of crazes and shearbands, and the conditions for the transition from one microdeformation mechanism to the other. Coextruded microlayers with many alternating layers of a crazing material and a shearbanding material are ideally suited for this purpose because of the large interfacial area and the variation that is possible in the layer thickness.

Microlayers of polycarbonate (PC) and styrene–acrylonitrile copolymer (SAN) combine a shearbanding material with a crazing one, and also exhibit the good interfacial adhesion required for stress transfer under conditions of high local strain. Deformation of this system has been studied in some detail in two dimensions, i.e. in thin sections taken through the thickness of sheets with many alternating layers [1–4]. The number of layers varied from 49 to 1857 in these studies, and the corresponding layer thicknesses varied from tens of micrometres to tenths of a micrometre. Interaction of SAN crazing with PC shearbanding was observed even with the thickest layers. As the layers were made thinner, co-operative phenomena and transitional behaviour became increasingly important; these were reflected macroscopically by increasing toughness [5].

Deformation of microlayer sheet has also been examined in the triaxial stress state at a semicircular notch. In addition to the interactive and co-operative microdeformation processes observed in thin sections, there were additional interactive phenomena that were unique to the triaxial condition [6–8]. To describe further the three-dimensional interaction of crazes and shearbands, optical microscopy and transmission electron microscopy were used to characterize the irreversible microdeformation mechanisms in microlayer sheet.

2. Experimental procedure

The microlayer composites with alternating layers of polycarbonate (PC) and styrene–acrylonitrile copolymer (SAN) were described previously [1]. Four compositions, all with 49 layers but differing in the ratio of PC to SAN, were chosen for the study. Individual

* *Present address:* Inteplast Corp., 1201 Formosa Drive, HWY 1593, Lolita, TX 77971, USA.
‡ To whom correspondence should be addressed.

0022–2461 © *1994 Chapman & Hall*

TABLE I Layer thickness and composition of microlayer composites

No. of layers	PC–SAN volume ratio		Total sample thickness (mm)	PC layer thickness[b] (μm)	SAN layer thickness[b] (μm)
	Given[a]	Measured[b]			
49	65/35	65/35	1.14	29.2	15.7
	54/46	62/38	1.08	27.1	16.6
	40/60	46/54	1.21	23.1	27.2
	27/73	28/72	1.15	12.8	32.9

[a] From extruder feed ratio.
[b] Average layer thickness and composition calculated from optical and SEM micrographs.

layer thicknesses were measured from optical micrographs and the results are summarized in Table I. The materials are described by the layer thicknesses rather than by the composition.

Microtensile specimens were tested in a miniature tensile tester mounted on the stage of an optical microscope as described previously [1]. The fixtures of the tensile tester were rotated so that the plane of the microlayers was viewed in the microscope, rather than the edges of the layers as in previous studies [1–4]. The focal plane was generally adjusted to the topmost SAN layer, although for comparison it was sometimes varied to focus on inner SAN layers.

For transmission electron microscopy, deformed specimens were cut into rectangular blocks about 1.5 mm in length with a low-speed diamond cutter. The blocks were affixed individually in capsules in the proper orientation before the capsules were filled with embedding resin and cured at room temperature for 24 h. The blocks were trimmed and sectioned with an ultramicrotome (RMC, MT6000-XL) at room temperature. The 100–200 nm thick sections were picked up on copper grids and examined in the transmission electron microscope (JEOL 100SX).

3. Results and discussion

3.1. Effect of layer thickness

Four microlayer compositions were chosen for the study. Because the composites were of similar total thickness and all had 49 alternating layers of PC and SAN, the individual PC and SAN layer thicknesses were determined by the PC–SAN volume ratio. The layer thicknesses measured by optical microscopy are summarized in Table I. The appearance of crazes and shearbands during tensile deformation at a speed of 0.3% min^{-1} is described in the following paragraphs.

3.1.1. SAN control

A typical stress–strain curve of the SAN control (Fig. 1a) was initially linear to a strain of about 1.8% when crazing initiated (Fig. 1b); crazing became more profuse as the stress increased (Fig. 1c). Crazes initiated from all the free surfaces, front and back as well as the edges. The crazes in Fig. 1b and c that do not touch either edge initiated from the front surface.

3.1.2. PC–SAN 13 μm/33 μm

A typical stress–strain curve of PC–SAN 13 μm/

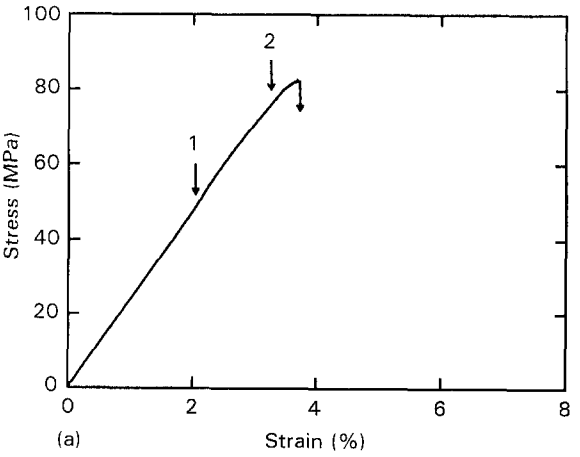

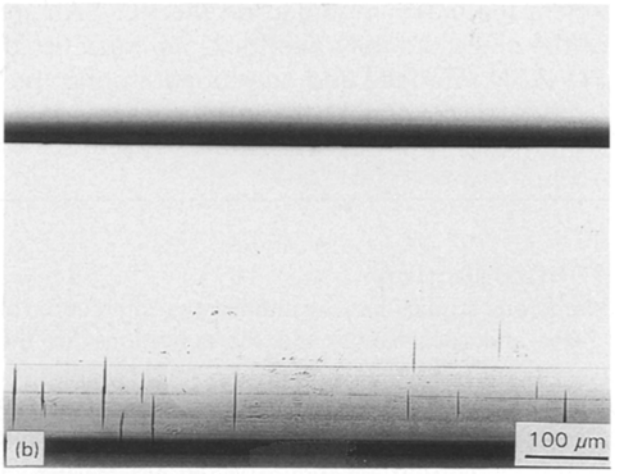

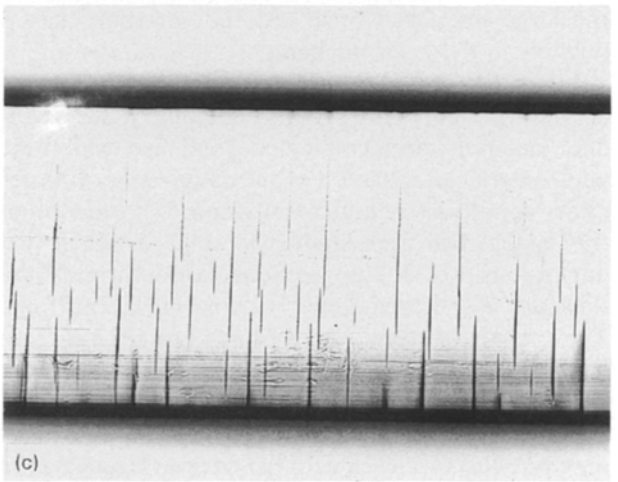

Figure 1 SAN control. (a) Typical stress–strain curve, arrows indicate strains at which optical micrographs in (b) and (c) were obtained: (b) 2.1% strain and (c) 3.5% strain. Test speed 0.03 mm min^{-1}.

33 μm (Fig. 2a) consisted of a linear region that extended to about 1.8% strain, when crazing was first observed, followed by a region of gradually decreasing slope. The fracture strain of 4.6% was somewhat higher than the 3.7% observed for the SAN control (Table II). The two arrows on the stress–strain curve identify the strains where optical micrographs illustrate deformation of the specimen. Crazes initiated from the edges at about 1.8% strain (Fig. 2b). The specimen in Fig. 2b was oriented so that the PC and SAN layers were stacked in the plane of the micrograph; because PC was the outer layer in all cases, the only free SAN surfaces from which crazes could initiate were the edges of the individual SAN layers. Each SAN layer crazed independently of the others; with crazes positioned throughout the depth, many were out of focus in transmission optical micrographs. At 4.2% strain, two things occurred virtually simultaneously: growth of the surface crazes terminated, and a second population of surface crazes initiated and tunnelled rapidly through the SAN layers (Fig. 2c). Each tunnel craze grew in a single SAN layer; most grew from one free surface to the other although a few terminated before reaching the other surface, probably because of local stress relief from other, nearby crazes. In this composition, there were many more tunnel crazes than surface crazes. Fracture occurred soon after the appearance of tunnel crazes.

Growth of several individual surface crazes as a function of strain is plotted in Fig. 3. The surface crazes slowly lengthened as the strain increased, reaching a maximum length of about 70 μm at 4.2% strain. New surface crazes continued to initiate as the strain increased from 1.8 to 4.2%. Once initiated, all the surface crazes lengthened at about the same rate, so that when growth of surface crazes ceased at 4.2% strain, the crazes that initiated at higher strains were shorter than the ones that initiated first. Examination of the fractured specimens revealed that the surface crazes often terminated in a pair of micro-shearbands in the SAN layer.

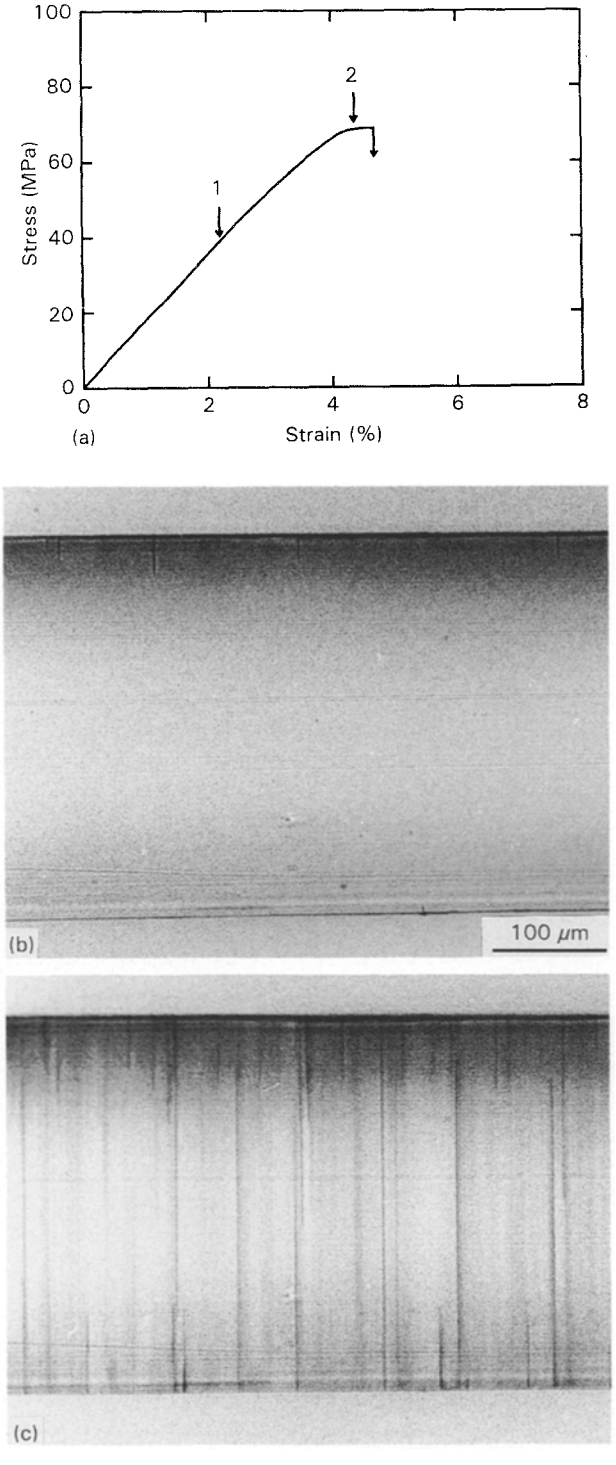

Figure 2 PC–SAN 13 μm/33 μm. (a) Typical stress–strain curve, arrows indicate strains at which optical micrographs in (b) and (c) were obtained: (b) 2.2% strain and (c) 4.4% strain. Test speed 0.03 mm min^{-1}.

TABLE II Tensile properties of SAN and PC–SAN microlayer composites[a]

Material	Fracture stress (MPa)	Fracture strain (%)	Yield stress (MPa)	Yield strain (%)
SAN	82.0	3.7	–	–
PC–SAN 13 μm/33 μm	69.0	4.6	–	–
PC–SAN 23 μm/27 μm	65.0	5.4	–	–
PC–SAN 27 μm/17 μm	63.0	5.4	–	–
PC–SAN 29 μm/16 μm	–	–	62.0	6.2

[a] Test speed: 0.03 mm min^{-1}.

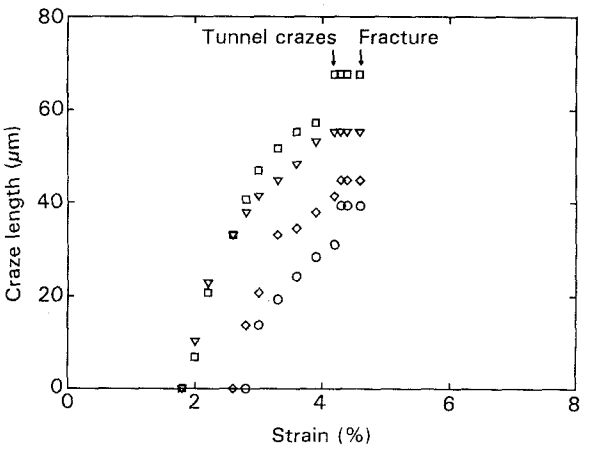

Figure 3 Length of individual surface crazes as a function of strain in PC–SAN 13 μm/33 μm.

3.1.3. PC–SAN 23 μm/27 μm

The representative stress–strain curve of this composition (Fig. 4a) resembled that of PC–SAN 13 μm/33 μm. The slightly lower initial slope, lower fracture stress and higher fracture strain reflected the higher PC content (Table II). Initiation of surface crazes in the SAN layers at 1.8% strain (Fig. 4b), gradual lengthening of the surface crazes with increasing strain, and termination of surface crazes at 4.2% strain with the appearance of tunnel crazes that extended from one free surface to the other (Fig. 4c) occurred in much the same way as described for the PC–SAN 13 μm/33 μm composite. The principal difference was the higher density of surface crazes in PC–SAN 23 μm/27 μm; additionally, craze-tip microshearbands were more distinct at the higher strains.

3.1.4. PC–SAN 27 μm/17 μm

A typical stress–strain curve of this composition (Fig. 5a) was very similar to that of PC–SAN 23 μm/27 μm. Crazing also closely resembled that of

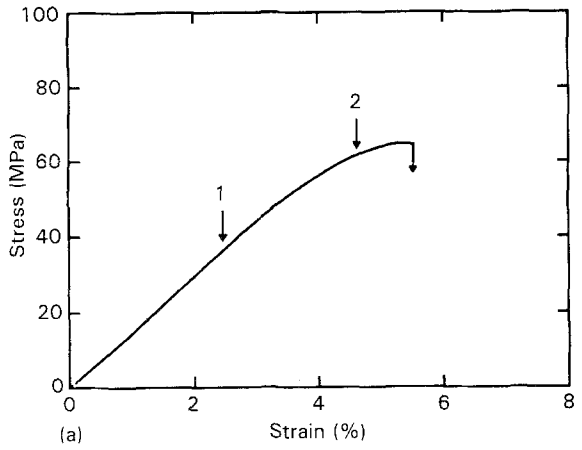

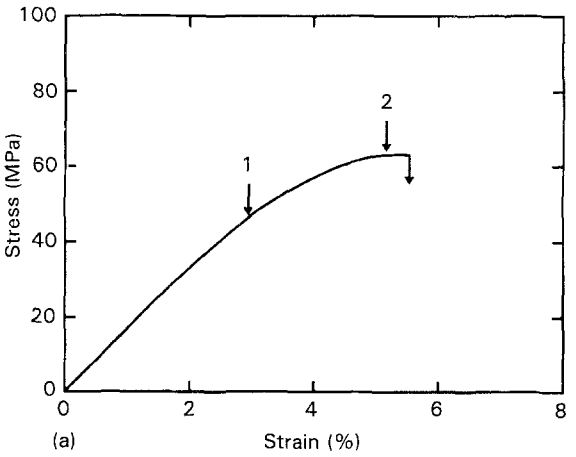

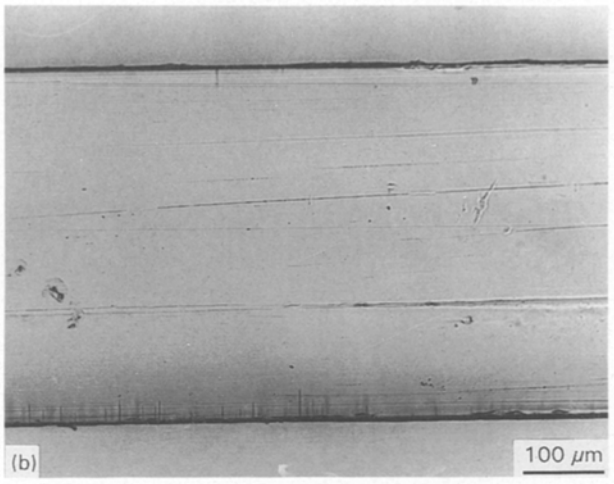

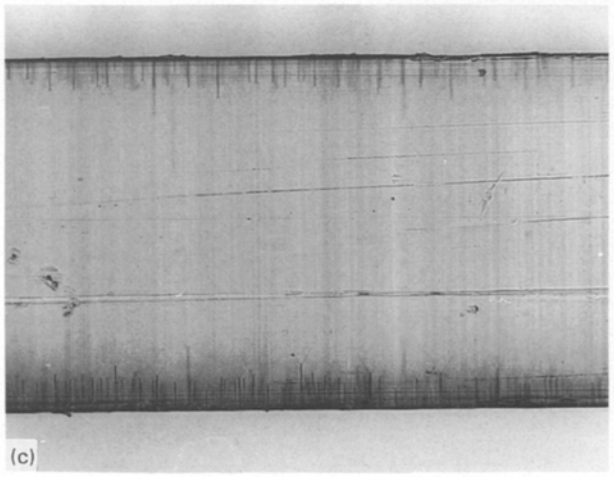

Figure 4 PC–SAN 23 μm/27 μm. (a) Typical stress–strain curve, arrows indicate strains at which optical micrographs in (b) and (c) were obtained: (b) 2.4% strain and (c) 4.7% strain. Test speed 0.03 mm min^{-1}.

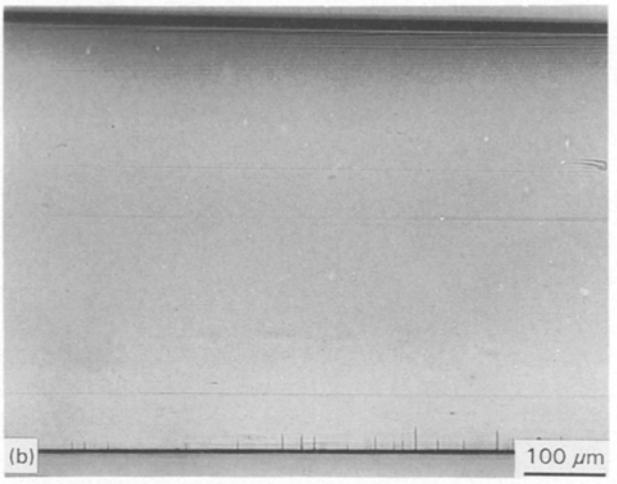

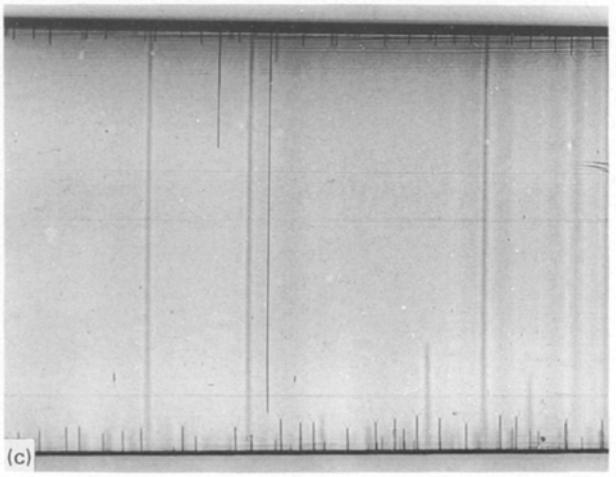

Figure 5 PC–SAN 27 μm/17 μm. (a) Typical stress–strain curve, arrows indicate strains at which optical micrographs in (b) and (c) were obtained: (b) 2.9% strain and (c) 5.3% strain. Test speed 0.03 mm min^{-1}.

the two compositions described previously, with the appearance and gradual growth of surface crazes between 1.8 and 4.2% strain (Fig. 5b). Craze-tip micro-shearbands appeared at 4.2% strain and tunnel crazes at 4.6% strain (Fig. 5c). The primary difference was the lower density of tunnel crazes and the slightly higher strain at which these appeared; most of the crazes were surface crazes in this composition.

Growth of several individual surface crazes as a function of strain is plotted in Fig. 6. As with the other compositions, the first crazes appeared at a strain of about 1.8% and lengthened until growth stopped at a strain of 4.2% when the longest surface crazes measured about 50 μm. After cessation of craze growth, micro-shearbands appeared at the craze tips. The shape of the growth curves and the final length of the surface crazes were the same in all microlayer compositions. The most significant difference was the increase in the density of surface crazes relative to tunnel crazes as the PC–SAN ratio increased. The stresses and strains at which the various microdeformation processes were observed are summarized in Table III for all the compositions.

Close examination of the optical micrographs suggested that growth of the surface crazes was terminated by a change in the mechanism of strain relief in the SAN layers from craze growth to initiation and growth of craze-tip micro-shearbands. The micrograph in Fig. 7 shows a pair of shearbands at the tip of each surface craze; the micro-shearbands grew out of the craze tip at an angle of 70–80° and prevented further lengthening of the surface crazes.

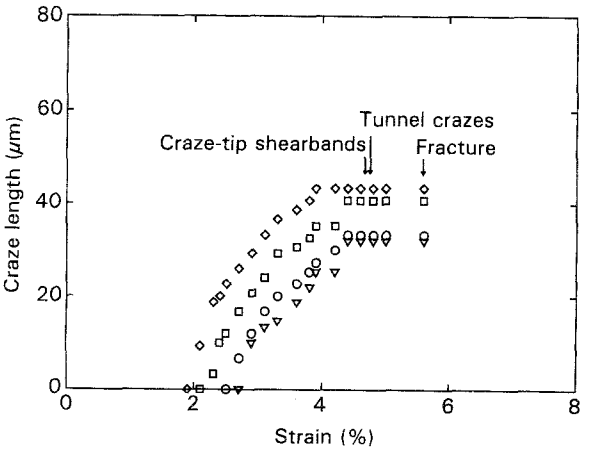

Figure 6 Length of individual surface crazes as a function of strain in PC–SAN 27 μm/17 μm.

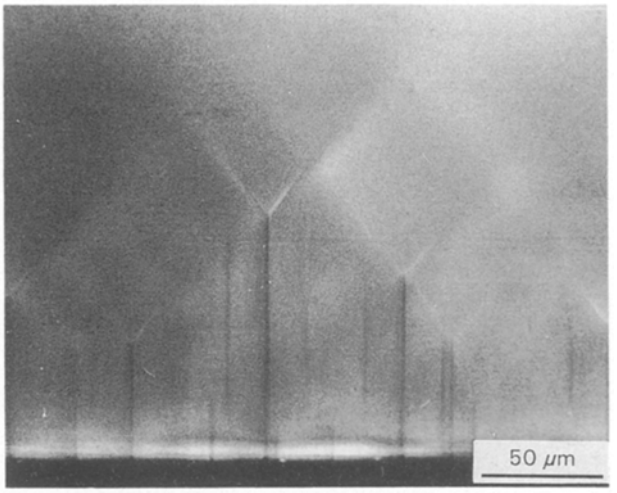

Figure 7 Higher magnification optical micrograph of surface crazes and craze-tip micro-shearbands in PC–SAN 27 μm/17 μm at 5.4% strain.

3.1.5. PC–SAN 29 μm/16 μm

This composition deformed in a ductile manner. Unlike the others, it yielded with formation and propagation of a stable neck (Fig. 8a). The yield stress and strain are included in Table II. The first observable deformation was again initiation of surface crazes at the free SAN surfaces, beginning at about 1.8% strain (Fig. 8b). Growth of the surface crazes ceased at about 4.2% strain when the longest crazes were about 60 μm. Micro-shearbands were clearly visible at the craze tips at 4.7% strain. No tunnel crazes were observed in this composition (Fig. 8c).

The surface crazes opened up when the specimen necked. Comparison of the surface crazes before and after necking (Fig. 9) showed that the crazes opened to many times their pre-necked width, while the depth of the opening extended only to the pre-necked depth where the craze was arrested by craze-tip micro-shearbands. After necking, most of the opened crazes exhibited an additional growth beyond the micro-shearbands, although this region did not open up in the same way as the original craze.

The 49 layer PC–SAN 29 μm/16 μm composition was used previously for in-depth studies of crazing in two dimensions, i.e. in thin sections taken through the thickness of the microlayer sheet [1–4]. It is now

TABLE III First appearance of surface crazes, SAN micro-shearbands and tunnel crazes in the edge view (*yz* plane)

Material	Surface crazes		SAN shearbands		Tunnel crazes	
	Stress (MPa)	Strain (%)	Stress (MPa)	Strain (%)	Stress (MPa)	Strain (%)
SAN Control	38.5	1.8	–	–	–	–
PC–SAN 13 μm/33 μm	32.6	1.8	71.4	4.5	71.2	4.2
PC–SAN 23 μm/27 μm	30.2	2.0	62.2	4.6	57.9	4.2
PC–SAN 27 μm/17 μm	24.7	1.7	60.6	4.7	63.8	4.8
PC–SAN 29 μm/16 μm	27.7	1.7	59.8	4.7	–	–

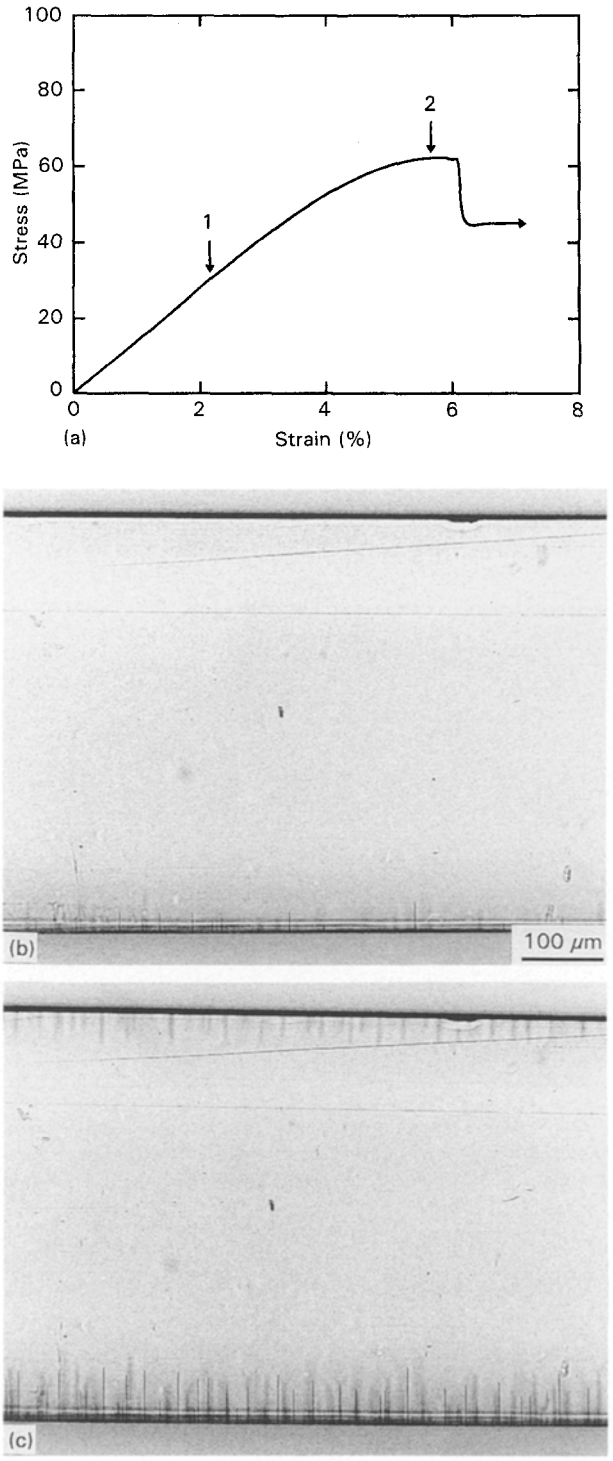

Figure 8 PC–SAN 29 μm/16 μm. (a) Typical stress–strain curve, arrows indicate strains at which optical micrographs in (b) and (c) were obtained: (b) 2.1% strain and (c) 5.6% strain. Test speed 0.03 mm min^{-1}.

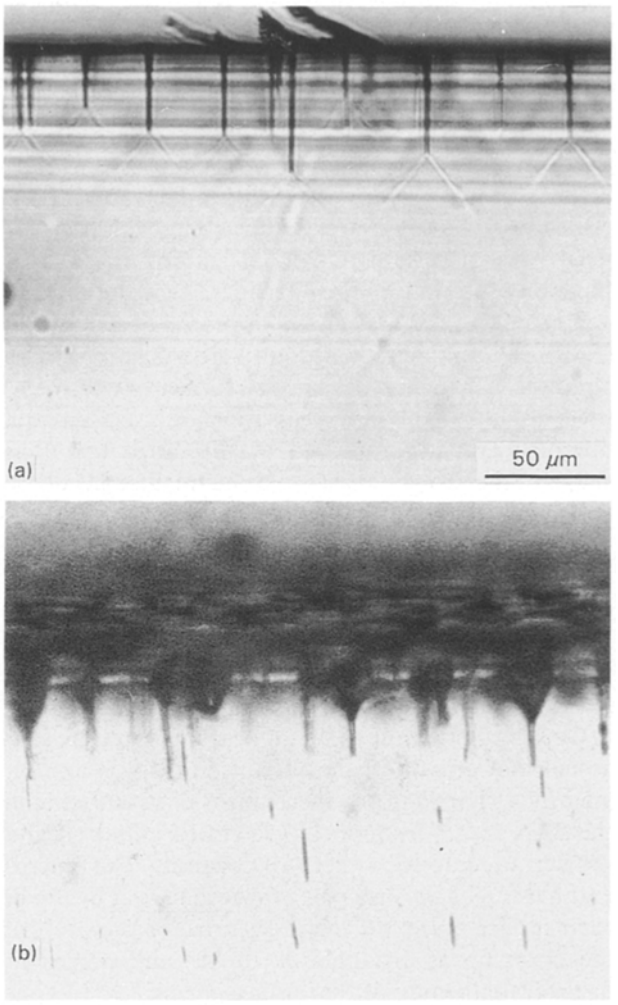

Figure 9 Surface crazes in PC–SAN 29 μm/16 μm. (a) Before necking and (b) after necking.

apparent that the findings of these studies pertain specifically to surface crazes. The additional insight into surface crazing that is provided by these studies relates to the statistical nature of the crazing; specifically, it can be stated that surface crazing occurs randomly in the SAN layers, and the increase in surface craze density with applied stress follows the Weibull distribution function [2]. Furthermore, the previous studies provide a detailed description and analysis of the plastic zone that forms in the PC layer as a result of impingement of the surface craze tip on the PC–SAN interface.

3.2. Strain rate effects, PC–SAN 29 μm/16 μm

When no tunnel crazes were observed in the PC–SAN 29 μm/16 μm composite at a speed of 0.3% min^{-1}, this composition was tested at several higher speeds of 1, 5 and 10% min^{-1}. Typical stress–strain curves are compared in Fig. 10. The initial slope and the yield strength increased slightly with the testing speed. The largest effect of test speed, however, was on the failure. At 1% min^{-1} the material failed in a ductile manner after localized necking and drawing; at 5% min^{-1} the material necked but fractured at 15% strain during neck propagation; and at 10% min^{-1} the specimen fractured at 5.8% strain without necking.

Surface crazes appeared at 1.8–2.0% at all strain rates. The microdeformation observed at 1% min^{-1} was very similar to that at 0.3% min^{-1}. Surface crazes initiated from the free SAN surfaces and reached a maximum length of 50 μm before they stopped growing at 4.2% strain; micro-shearbands were visible at the craze tips at 4.5% strain. No tunnel crazes were observed at this test speed (Fig. 11a). When the specimen necked, the surface crazes opened up but did not propagate in the thickness direction. An effect of strain rate was seen in the decreasing number of surface crazes at 5 and 10% min^{-1}. Tunnel crazes were also observed at 5% min^{-1}, and the number of tunnel

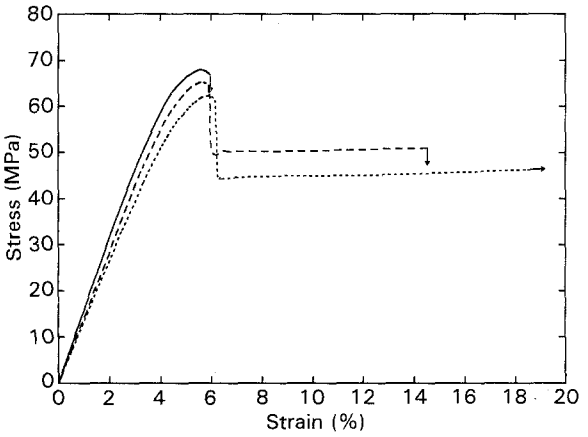

Figure 10 Typical stress–strain curves of PC–SAN 29 μm/16 μm at strain rates of (– – –) 1% min^{-1}, (— —) 5% min^{-1} and (——) 10% min^{-1}.

crazes increased at 10% min^{-1}. The surface crazes that did initiate when the test speed was 5% min^{-1} grew to a maximum length of only 30 μm before they were terminated by micro-shearbands. When the strain reached 4.5%, numerous tunnel crazes initiated and rapidly propagated through the SAN layers from one free surface to the other (Fig. 11b). Despite the tunnel crazes, a stable neck formed at this strain rate. The short surface crazes were pulled open during necking; subsequently, a crack that initiated from the opened surface crazes caused catastrophic fracture during neck propagation. At the highest speed, 10% min^{-1}, only a few surface crazes were observed. Instead, many tunnel crazes appeared before the specimen fractured without necking at a strain of 5.8% (Fig. 11c).

3.3. Morphology of surface crazes and micro-shearbands

3.3.1. Morphology in the xy *plane*

Morphology of surface crazes was examined in the PC–SAN 29 μm/16 μm composition. Fig. 12a shows a surface craze from a strained specimen before it necked. The wedge-shaped craze was about 1.1 μm wide at the surface and gradually tapered off toward the craze tip. The microfibrils bridging the craze were about 20 to 150 nm wide which is in the range reported in the literature [9]. A pair of very fine micro-shearbands could be discerned growing out from the craze tip. The rather large angle of the micro-shearbands, 95–100°, was due to compression of the section during microtoming.

A similar section of a surface craze in the necked region is shown in Fig. 12b. The craze had opened up widely; near the surface where the craze was widest the craze fibrils fractured, while closer to the tip of the craze the fibrils remained intact. A pair of micro-shearbands was faintly visible curving away from the position of the original craze tip. To accommodate the craze opening without further craze growth, material in the region of the craze tip was required to undergo large plastic deformation. The large shear strains this required of SAN evolved from these micro-shear-

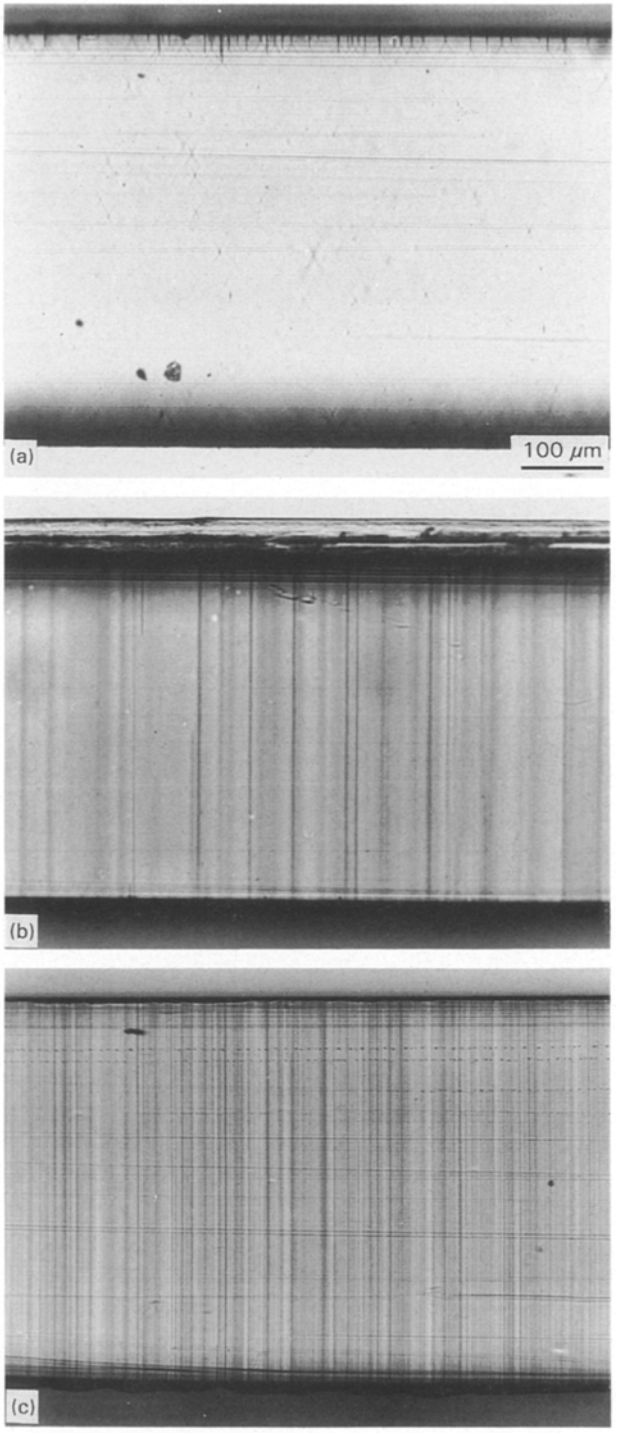

Figure 11 Optical micrographs of PC–SAN 29 μm/16 μm deformed at various strain rates: (a) 1% min^{-1}, 5.7% strain; (b) 5% min^{-1}, 5.7% strain; (c) 10% min^{-1}, 5.8% strain.

bands. When plastic deformation of the SAN could not totally accommodate the craze opening, a small crack started to grow from the original craze tip. Ultimately, catastrophic fracture initiated from these opened crazes.

3.3.2. Morphology in the yz *plane*

The edge of a tensile specimen after it had been deformed almost to the neck instability is shown in Fig. 13. Viewed in this orientation, the surface crazes appeared as dark lines that extended across the individual SAN layers. As indicated previously, crazes

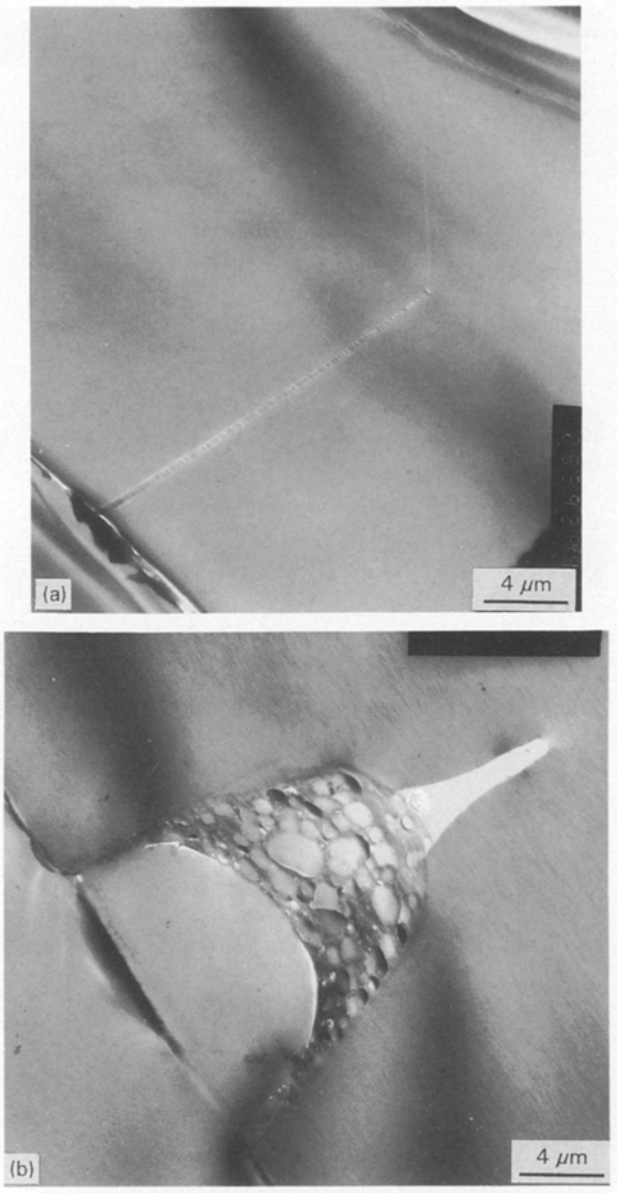

Figure 12 Transmission electron micrographs of surface crazes in thin *xy* sections of PC–SAN 29 μm/16 μm. (a) Before necking and (b) after necking.

initiated randomly in the SAN layers with no registry from one SAN layer to the next [2]. Micro-shearbands were visible at the craze tips. The micro-shearbands seen in this orientation were in the PC layers; they originated near the PC–SAN interface where the craze tips impinged on the neighbouring PC layers. The stresses and strains at which crazes and PC micro-shearbands were observed in this orientation are summarized in Table IV. The craze initiation strain was the same in both orientations, 1.8–2.0%; however, micro-shearbands in the PC layers were observed at a slightly lower strain, about 4.2%, than the craze-tip micro-shearbands in the SAN layers, about 4.6–4.7%.

The optical micrograph in Fig. 13a shows the edge of a specimen after it was sectioned to a depth of 20 μm, and the same region is shown again in Fig. 13b after the specimen was sectioned to a depth of 60 μm. Crazes that originally were shorter than 60 μm are no longer visible, and only those that originally were

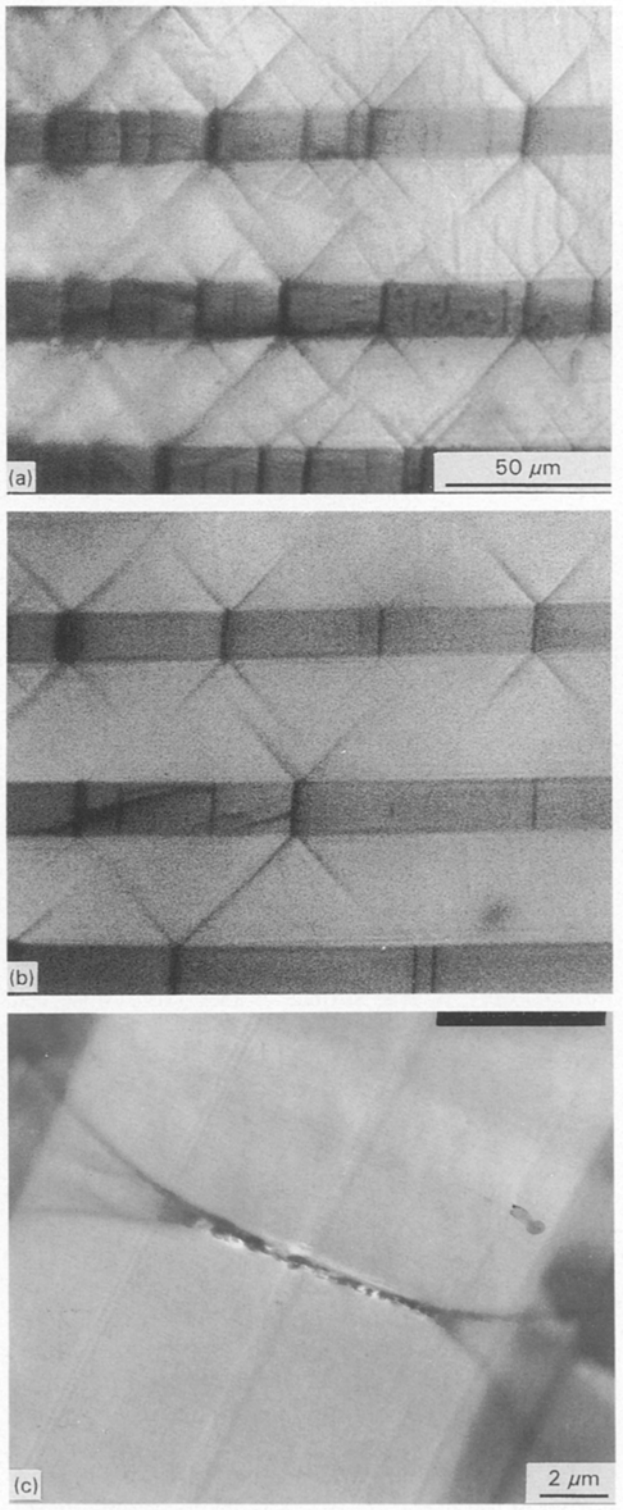

Figure 13 PC–SAN 29 μm/16 μm deformed almost to the neck instability and viewed in the *yz* plane. (a) Optical micrograph of the block microtomed to a depth of 20 μm; (b) optical micrograph of the same region of the block microtomed to a depth of 60 μm; (c) transmission electron micrograph of a thin section microtomed from the block at a depth of about 40 μm.

longer than 60 μm are still present. Most of these span the width of the SAN layer. A few of the crazes do not reach the layer interface; these crazes were sectioned close to the craze tip and do not extend to the interface because the craze tip was slightly curved.

Fig. 13c is a TEM micrograph of one of the thin sections removed from the specimen in Fig. 13b and shows a craze that did not extend to the interface at

TABLE IV First appearance of crazes and PC micro-shearbands in the front view (xy Plane)

Material	Crazes		PC micro-shearbands	
	Stress (MPa)	Strain (%)	Stress (MPa)	Strain (%)
PC–SAN 13 μm/33 μm	32.3	2.0	66.5	4.1
PC–SAN 23 μm/27 μm	27.4	1.9	57.5	4.2
PC–SAN 27 μm/17 μm	24.1	1.7	55.5	4.1
PC–SAN 29 μm/16 μm	26.1	1.9	53.4	4.1

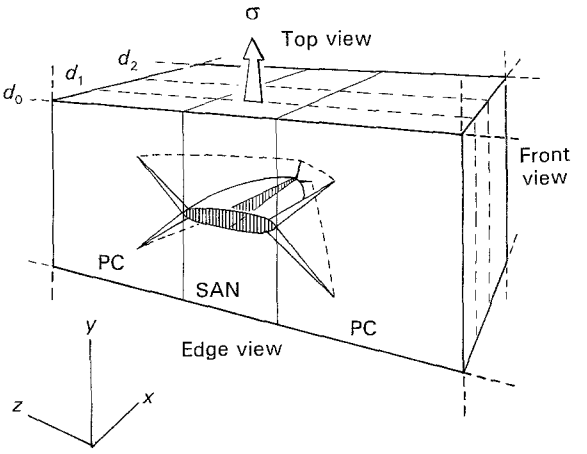

Figure 14 Three-dimensional model of a surface craze with micro-shearbands in PC–SAN 29 μm/16 μm.

higher magnification. The line of cavitation defines the cross-section of the craze; a pair of micro-shearbands begins at each tip and extends through the uncrazed portion of the SAN layer and smoothly across the interface into the PC layer. Apparently the micro-shearbands in the adjacent PC layers induced a transition in the SAN from craze growth to shearing. The shearband angle of 60–65° is smaller than in the optical micrographs, probably because of compression during microtoming since the cutting direction was perpendicular to the layers.

3.3.3. A three-dimensional model of surface crazes and micro-shearbands

A three-dimensional model of the surface craze was derived from the micrographs. The surface craze sketched in Fig. 14 is based on observations of the PC–SAN 29 μm/16 μm composition but is general for surface crazes in all the PC–SAN microlayer composites. In the edge view (yz plane) the craze opening is somewhat greater in the centre than at the interface with the neighbouring PC layer, which gives the craze a slightly oval cross-section. Micro-shearbands have initiated in the neighbouring PC layers where the craze tips impinge on the PC–SAN interface, and have grown some distance into the PC layers. In the front view (xy plane) the craze is wedge-shaped, tapering to the tip where it terminates in a pair of micro-shearbands in the SAN layer. The micro-shearbands enclose the craze by extending continuously from one PC layer to the other through the SAN layer. The micro-shearband angle appears to change slightly from 83 ± 3° in PC to 73 ± 3° in SAN.

The postulated progression of surface crazing and micro-shearbanding with increasing strain is sketched in Fig. 15. Crazes initiate at the free surfaces of the SAN layers beginning at 1.8% strain and slowly

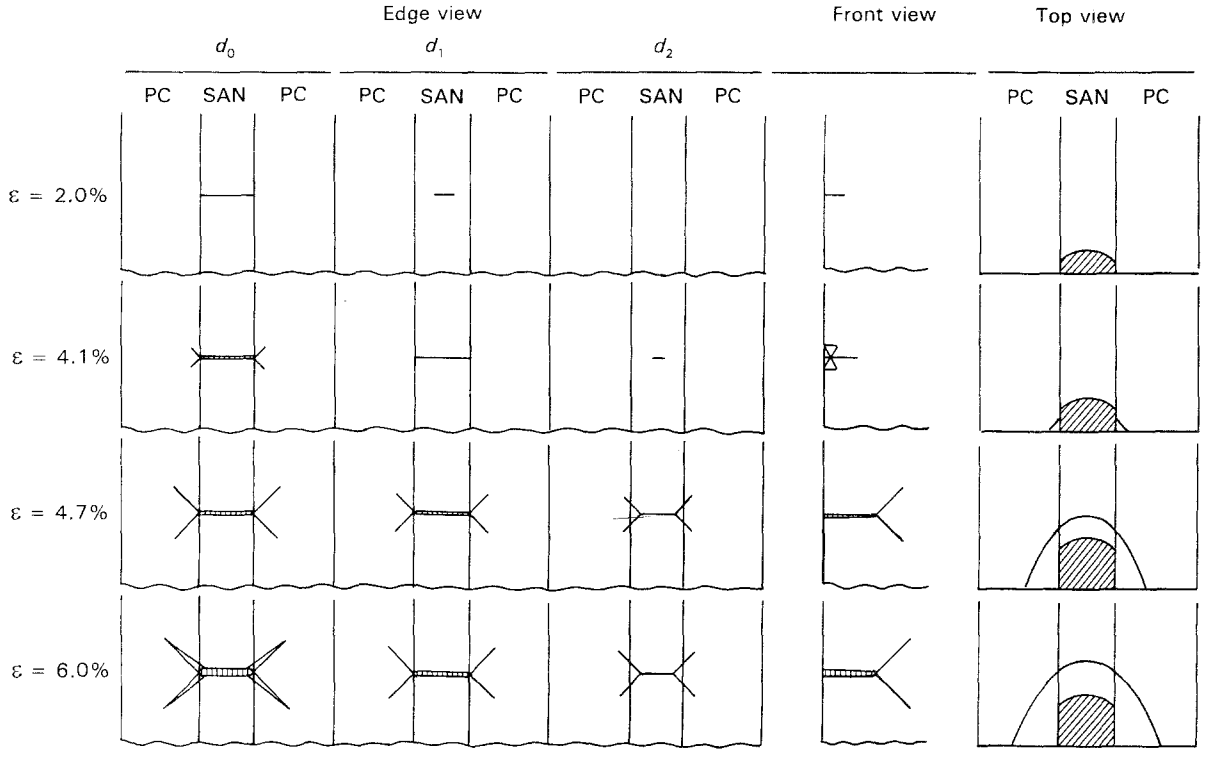

Figure 15 Sketches showing interactive craze and micro-shearband growth in the three orthogonal planes. (a) Edge view (yz plane) at several depths; (b) front view (xy plane); (c) loading plane (xz plane).

lengthen as the strain increases. Micro-shearbanding is first observable in the optical microscope at 4.2% strain when it is seen in the PC layers. In contrast, micro-shearbands are not detected at the craze tip until the strain reaches 4.7%. It appears that micro-shearbands form first at the surface in the PC layers in response to the stress concentration created by impingement of the craze tip on the PC–SAN interface. The shearbands lengthen away from the interface into the PC layer as the strain increases; they also follow the edge of the craze along the PC–SAN interface. Once initiated, the micro-shearbands grow faster than the craze and rapidly overtake the craze tip. As they approach the curved craze tip where the craze does not reach the interface, it is possible for the micro-shearbands to penetrate through the PC–SAN interface and propagate around the craze tip to entirely engulf the craze. This terminates craze growth, and further strain in the SAN layer is accommodated by shear deformation.

It appears inconsistent that termination of craze growth is observed at 4.2% strain, while micro-shearbands are not detectable at the craze tips until the strain reaches 4.7%. The description in Fig. 15 is based on optical microscope observations, and the actual onset of shear deformation would have preceded observable micro-shearbands. Once micro-shearbands initiated in the PC layers at 4.2% strain, shear deformation probably propagated quite rapidly along the edge of the craze to engulf the craze tip.

4. Conclusions

Previous understanding of two-dimensional interactive crazing and shearbanding in microlayers of PC and SAN has been extended to include the third direction. The observations are summarized as follows:

1. Two types of SAN crazes are seen. Crazes first initiate at the free surface of the SAN layers at 1.8% strain and slowly lengthen until their growth terminates at a strain of 4.2% when the maximum length is about 60 μm. The second type of craze is observed at strains greater than 4.2%. These crazes also initiate at the free surface of the SAN layers but then tunnel rapidly through the SAN layer from one free surface to the other.

2. A transition from predominately surface crazing to predominately tunnel crazing occurs as the PC–SAN layer thickness ratio is decreased, or as the strain rate is increased. Surface crazes do not prevent localized yielding and stable neck propagation, while tunnel crazes are associated with loss of ductility.

3. The local stress concentration created by the surface craze produces micro-shearbanding in neighbouring PC layers where the craze impinges on the PC–SAN interface. The interactive micromechanics also cause a transition from crazing to micro-shearbanding in the SAN layer when a pair of micro-shearbands appear at the tip of the growing craze.

4. A three-dimensional model of interactive surface crazing and micro-shearbanding is proposed in which micro-shearbands initiate first in the PC layers and propagate rapidly along the edges of the craze. When they overtake the craze tip, the micro-shearbands penetrate through the PC–SAN interface and continue around the craze tip to entirely engulf the craze. This terminates craze growth, and further strain in the SAN layer is accommodated by shear deformation.

Acknowledgements

The authors thank Dr J. Im of the Dow Chemical Company for many helpful technical discussions, and the Dow Chemical Company, Midland, MI, for supplying the co-extruded microlayers. For continuing financial support, the authors thank the National Science Foundation, Polymers Program (91-00300).

References

1. D. HADERSKI, K. SUNG, J. IM, A. HILTNER and E. BAER, *J. Appl. Polym. Sci.* **52** (1994) 121.
2. K. SUNG, D. HADERSKI, A. HILTNER and E. BAER, *ibid.* **52** (1994) 135.
3. *Idem, ibid.* **52** (1994) 147.
4. M. MA, K. VIJAYAN, J. IM, A. HILTNER and E. BAER, *J. Mater. Sci.* **25** (1990) 2039.
5. J. IM, E. BAER and A. HILTNER, in "High Performance Polymers", edited by E. Baer and A. Moet (Hanser, New York, 1991) p.175.
6. E. SHIN, A. HILTNER and E. BAER, *J. Appl. Polym. Sci.* **47** (1992) 245.
7. *Idem, ibid.* **47** (1992) 269.
8. A. HILTNER, K. SUNG, E. SHIN, S. BAZHENOV, J. IM and E. BAER, *Mater. Res. Soc. Symp. Proc.* **255** (1992) 141.
9. G. H. MICHLER, *J. Mater. Sci.* **25** (1990) 2321.

Received 7 March
and accepted 22 April 1994